Analysis of uncertainties in α-particle optical-potential assessment below the Coulomb barrier

V. Avrigeanu* and M. Avrigeanu
Horia Hulubei National Institute for Physics and Nuclear Engineering, P.O. Box MG-6, 077125 Bucharest-Magurele, Romania
(Received 8 April 2016; published 30 August 2016)

Background: Recent high-precision measurements of α-induced reaction data below the Coulomb barrier have pointed out questions about the α-particle optical-model potential (OMP) which are still unanswered within various mass ranges.
Purpose: The applicability of previous optical potential and eventual uncertainties and/or systematic errors of the OMP assessment at low energies can be further considered on this basis.
Method: Nuclear model parameters based on the analysis of recent independent data, particularly γ-ray strength functions, have been involved within statistical model calculation of the (α,x) reaction cross sections.
Results: The above-mentioned potential provides a consistent description of the recent α-induced reaction data with no empirical rescaling factors of the γ and/or nucleon widths.
Conclusions: A suitable assessment of α-particle optical potential below the Coulomb barrier should involve the statistical-model parameters beyond this potential on the basis of a former analysis of independent data.

DOI: 10.1103/PhysRevC.94.024621

I. INTRODUCTION

Recent high-precision measurements [1–6] of α-particle-induced reaction data below the Coulomb barrier (B) provide a useful opportunity to investigate the results of a previous optical-model potential (OMP) for α particles on nuclei within the mass number range $45 \leqslant A \leqslant 209$ [7]. Actually, this potential was established by (1) analysis of α-particle elastic-scattering angular distributions above B [7,8] and (2) Hauser-Feshbach statistical model (SM) assessment of the available (α,γ), (α,n), and (α,p) reaction cross sections for incident energies below B and target nuclei with $A \leqslant 120$ [9] or heavier [7,10]. Thus, starting from a semimicroscopic OMP with a double-folding model (DFM) real part and a phenomenological energy-dependent imaginary-potential dispersive contribution [8,9], a full phenomenological analysis of the same data led to a spherical OMP to be easily involved within SM calculations for basic and applied objectives. The main points of this potential are (i) a strongly modified energy dependence of the surface imaginary-potential depth below $0.9B$ [9], which is now a reference energy in this respect (e.g., Ref. [12]) and (ii) an energy-dependent radius of the surface imaginary part for the well-deformed nuclei [7].

A consistent description of all α-induced reaction data available at that time [7,9,10] was provided using this potential and especially no empirical rescaling factors of the γ and/or neutron widths. However, the above-mentioned recent works have pointed out α-particle OMP questions yet open within various mass ranges. Thus, a detailed systematic study of the (α,γ) reactions for all stable nickel isotopes [1], following also recent distinct studies of this reaction on ^{58}Ni [13] and ^{62}Ni [14] isotopes, aimed to provide a constraint for the choice of input models in a given A range. Nevertheless, different best combinations of input parameters for the TALYS 1.6 code [15] were found for each of the investigated isotopes while the combination identified that reproduces simultaneously the experimental data for all Ni isotopes has been at variance with the findings of the distinct studies [13,14] as well as the grounds of the concerned α-particle OMP [16]. Actually, the particular study of the ^{58}Ni$(\alpha,\gamma)^{62}$Zn reaction had already mentioned that further theoretical work is required to obtain a full understanding of α-induced reaction data on ^{58}Ni [13].

The (α,n) and (α,γ) reaction cross sections of several proton-rich nuclei within the region just above the $A \approx 100$ form also the object of several recent studies at low energies, with similar results for the reliability of SM predictions. So, it was possible to reproduce simultaneously the data for ^{107}Ag only by rescaling the ratio of γ to neutron widths [2]. A study of both elastic-scattering and α-induced reaction cross sections for ^{106}Cd at low energies concluded as well that these data constrain the other SM ingredients except the α-particle OMP [3]. Total and partial cross sections of the (α,γ) reaction, measured for the first time, for ^{112}Sn target nucleus pointed out a disagreement between experiment and theory which was considered to be most probably a deficiency of the nuclear-physics input [4].

The (α,n) reaction cross-section studies performed in the meantime also for the heavier nuclei ^{164,166}Er [5] and ^{187}Re [6], with the main goal to test the low energy modification [11,12] of the widely used α-particle OMP of McFadden and Satchler [17], concluded that the corresponding energy dependence steepness assumed for a Fermi-type volume imaginary potential has different parameter values of 2.5 and 4 MeV, respectively. Moreover, it has been considered an open question [2,3,5,6] whether this modification is due to a required OMP change, which affects the total reaction cross section, or due to neglecting the Coulomb excitation (CE) in the entrance channel [18]. All these newly measured data and related α-particle OMP studies within different mass ranges motivated the present work, with the aim to both check the applicability of the previous OMP [7] and to look for uncertainties and possible systematic errors of α-particle optical-potential assessment at low energies.

*vlad.avrigeanu@nipne.ro

Contrary to the conclusions of the above-mentioned studies of α-particle-induced reaction data at low energies, obtained on the basis of these data fit using a range of global input parameters for the SM calculations, we pay attention first to the use of a consistent input parameter set, either established or validated by analyzing various independent data. This set is briefly described in Sec. II of this work, while more detailed presentation was given previously [7,19,20]. The results corresponding to the OMP of Ref. [7] are then compared with the recently measured cross sections [1–6] in Sec. III, followed by conclusions in Sec. IV.

II. NUCLEAR MODELS AND PARAMETERS

A. Coulomb excitation effects on α-particle OMP setting up

The overestimation of the α-induced reaction cross sections at low energies provided by the use of the α-particle OMP of McFadden and Satchler [17] has been explained recently [18] by the neglect of the CE process, i.e., the α-particle inelastic scattering by the electric field of the target nucleus. Consequently, the CE diversion of the incident flux from the compound-nucleus (CN) channel was taken into account by decreasing the OMP transmission coefficients given for each partial wave. Because the corresponding renormalization of the α-particle total-reaction cross section σ_R does not affect the α-particle emission, the CE effects in the incident channel have been considered at the origin of the difference between the OMPs corresponding to the incident and emitted α particles, respectively [18].

However, following former comments on this assumption [7] and detailed CE calculations [21,22], it has been shown that the corresponding partial waves and integration radii provide evidence for the distinct account of the CE cross section and OM σ_R [23]. Thus the largest contribution to CE cross section comes by far from partial waves larger than the ones contributing to the σ_R values. Nevertheless, in nuclear reaction model calculations one should pay attention only to the assessment of direct-interaction (DI) collective α-particle inelastic scattering cross section, which should be subtracted from α particle σ_R in order to obtain the corresponding CN cross section, which is to be then involved in statistical model calculations. The point is that only the effects of the CE+nuclear interference that correspond to an integration radius which is typical to the short-range nuclear interactions, i.e., of ∼15 fm, should be considered in this respect. On the other hand, the cross sections related to these effects are usually much lower than the σ_R values even below B [23], so that they can be omitted in a first instance.

B. Statistical model parameters

We have also used within the present (α,x) reaction analysis a consistent set of (i) nucleon [24] and (ii) γ-ray transmission coefficients, and (iii) back-shifted Fermi gas (BSFG) nuclear level densities [25]. They have been established or validated on the basis of independent measured data for neutron total cross sections and (p,n) reaction cross sections [26], γ-ray strength functions [27–36] and (p,γ) reaction cross sections [26], and low-lying levels [37] and resonance data [38], respectively. Only the points in addition to the details given formerly [7,19,20] as well as the particular parameter values are mentioned hereafter.

The SM calculations discussed in the following were carried out mostly within a local approach using an updated version of the computer code STAPRE-H95 [39], with ∼0.2-MeV equidistant binning for the excitation energy grid. The latest version 1.8 of the code TALYS [15] has also been used in the particular case of the ^{187}Re$(\alpha,n)^{190}$Ir reaction. The presently calculated reaction cross sections have been compared elsewhere [40] with the content of the TALYS-based evaluated data library TENDL-2015 [41], too, for an overall excitation function survey.

1. Nuclear level densities

The BSFG model parameters used in the following SM calculations are given in Table I, following the low-lying levels numbers and excitation energies [37] used in the SM calculations (the second and third columns), as well as the independent data that have been involved in their setting up for the nuclei with $A \sim 60$, $A \sim 110$, and $A \sim 160$, in addition to the parameters and data given formerly within Refs. [20], [19], and [7], respectively, or in the case of BSFG parameter updates. These updates, particularly for ^{61,63}Cu and $^{64-68}$Zn nuclei, concern changes between 0.6 and 3% for the level density parameter a, with corresponding changes of the g.s. shift Δ in order to fit the low-lying levels and resonance data given in this table. They followed either the availability of new data [37] published in the meantime, or the increased attention paid to the accurate account of Zn isotopes, which have been of larger interest now than previously [20]. Actually, the data in Table I are given not as results of a basic nuclear level density study but to provide the reader with all main details of the present analysis.

2. Optical model potentials

The neutron optical potential of Koning and Delaroche [24] was obviously the first option, however, paying the due attention to the authors' remark that their global potential does not reproduce the minimum around the neutron energy of 1–2 MeV for the neutron total cross sections σ_T of the $A \sim 60$ nuclei. In spite of the scarce σ_T database available for the Zn isotopes [26], we found that the global potential [24] provides a suitable description of these data for the neutron energies starting from 2 MeV, while there is an ∼40% overestimation for the energies below 1 MeV. Because the latter energy range is most important for the statistical CN de-excitation within the (α,x) reactions below B, we looked for a better description of this energy range. Thus we found that the σ_T values calculated by using the simplified local potential of Engelbrecht and Fiedeldey [43] are in good agreement with the experimental data. Therefore we involved this neutron OMP in the SM calculations for Ni isotopes while, following the results shown in Sec. III A, the global potential [24] was used in the rest of this work.

The proton optical potential of Koning and Delaroche [24] was also first considered for the calculation of the proton transmission coefficients, too. A particular check was found, however, to be desirable for the residual Cu isotopes because

TABLE I. Low-lying levels number N_d up to excitation energy E_d^* [37] used in reaction cross-section SM calculations, the low-lying levels and s-wave nucleon-resonance spacings $D_0^{\rm exp}$ (with uncertainties given in parentheses, in units of the last digit) in the energy range ΔE above the separation energy S, for the target-nucleus ground state (g.s.) spin I_0, fitted to obtain the BSFG level-density parameter a and g.s. shift Δ (for a spin cutoff factor calculated with a variable moment of inertia [42] between half and 75% of the rigid-body value, from g.s. to S, and reduced radius $r_0 = 1.25$ fm), and the average radiation widths Γ_γ, either measured [38] or based on systematics (given between square brackets), and corresponding to the SLO, GLO, and EGLO models, with the parameter $T_f = 0.7$ MeV being used for description of the RSF data of the Zn isotopes [27–33,36] by the EGLO model.

Nucleus	N_d	E_d^*	Fitted low-lying levels and nucleon-resonance data						a	Δ	Γ_γ		
		(MeV)	N_d	E_d^* (MeV)	$S+\frac{\Delta E}{2}$ (MeV)	I_0	$D_0^{\rm exp}$ (keV)	Γ_γ (meV)	(MeV^{-1})	(MeV)	SLO (meV)	GLO (meV)	EGLO (meV)
^{58}Ni	34	4.574	34	4.574					5.90	0.40			
^{60}Ni	50	4.579	51	4.613					6.00	0.06			
^{61}Ni	35	2.863	35	2.863	8.047	0	13.8(9)[a]	1120(200)	6.55	−0.93			
^{62}Ni	46	4.455	46	4.455	10.631	3/2	2.10(15)[a]	2000(500)	6.36	0.27			
^{64}Ni	20	3.849	51	4.613					6.90	0.75			
^{61}Cu	36	3.042	38	3.092					6.75	−0.64			
^{63}Cu	60	3.291	105	3.92	9.026	0	5.9(7)[a]		7.00	−0.65			
^{64}Cu	40	1.780	40	1.780	7.993	3/2	0.70(9)[b]	490(30)	7.70	−1.55			
^{65}Cu	40	3.132	48	3.278					7.85	−0.10			
^{66}Cu	22	1.439	22	1.439	7.116	3/2	1.30(11)[a]	385(20)	7.88	−1.40			
^{67}Cu	6	1.937	5	1.670					8.20	0.07			
^{61}Zn	15	1.730	15	1.730					6.70	−1.25			
^{62}Zn	32	4.217	32	4.217	12.890	3/2		[730(330)]	6.20	0.16	2920	2080	1380
^{63}Zn	21	1.978	20	1.909					7.50	−0.93			
^{64}Zn	60	3.993	75	4.319	11.862	3/2		[510(230)]	6.80	−0.04	1760	1370	740
^{65}Zn	35	2.216	35	2.216	8.018	0	2.3(3)[a]	726(60)	8.33	−0.71	445	280	200
^{66}Zn	33	3.738	39	3.825	11.059	5/2		[450(180)]	7.70	0.55	740	475	290
^{67}Zn	40	2.175	40	2.175	7.278	0	4.62(55)[a]	390(60)	8.11	−0.97			
^{68}Zn	51	3.943	51	3.943	10.291	5/2	0.37(2)[a]	440(60)	8.05	0.59	1260	860	460
^{107}Ag	19	1.325	19	1.325					13.70	−0.23			
^{105}Cd	8	0.771	11	0.832				[187(94)]	12.60	−0.54	439	341	106
^{106}Cd	22	2.566	24	2.630				[300(150)]	13.00	0.86	511	372	129
^{110}Cd	36	2.662	38	2.707					13.75	0.82			
^{111}Cd	42	1.346	42	1.346	6.979	0	0.155(20)[a]	71(6)	13.84	−0.58	223	185	59
^{112}Cd	25	2.507	25	2.507	9.399	1/2	0.027(3)[a]	106(15)	13.81	0.82	315	244	77
^{109}In	17	1.816	16	1.759					14.00	0.29			
^{110}In	25	1.006	30	1.063					14.50	−0.61			
^{111}In	36	2.112	36	2.112	9.992	7.0		[180(60)]	14.40	0.35	500	360	125
^{109}Sn	13	1.269	13	1.269					13.90	−0.12			
^{110}Sn	30	3.183	30	3.183	11.270	5/2		[180(90)]	13.40	1.35	461	263	115
^{112}Sn	23	2.986	23	2.986					13.85	1.34			
^{116}Sn	17	2.844	26	3.106				[120(30)]	13.45	1.33	226	185	76
^{117}Sn	22	1.628	22	1.628	6.945	0	0.45(5)[a]	52(5)	13.40	−0.08	216	185	60
^{118}Sn	38	3.057	38	3.057	9.326	1/2	0.061(7)[a]	117(20)	13.45	1.10	291	227	76
^{119}Sn	24	1.633	24	1.633	6.485	0	0.700(15)[a]	45(7)	13.50	−0.13	169	150	39
^{121}Sn	20	1.450	20	1.450	6.171	0	1.25(20)[a]	40(5)	13.00	−0.30	169	154	27
^{122}Sn	21	2.780	21	2.780				[85(42)]	13.40	1.08	263	194	47
^{115}Sb	15	2.104	15	2.104					14.00	0.65			
^{115}Te	8	1.272	8	1.272					14.00	0.09			
^{116}Te	8	1.812	8	1.812	11.278	7/2		[295(20)]	14.00	0.63	1150	562	290
^{164}Er	39	1.766	39	1.766					17.00	0.16			
^{167}Tm	26	0.631	26	0.631					18.20	−0.77			
^{167}Yb	30	0.571	34	0.628					18.50	−0.83			
^{168}Yb	28	1.551	28	1.551	9.062	5/2		[110(30)]	17.50	0.11	420	578	150
^{187}Re	34	1.003	34	1.003					19.50	−0.37			
^{190}Os	34	1.708	34	1.708	7.792	3/2	0.0034(4)[a]		19.40	0.32			
^{190}Ir	26	0.287	26	0.287					19.70	−0.13			
^{191}Ir	20	0.686	20	0.686					19.50	−0.53			

[a]Reference [38]
[b]Reference [25]

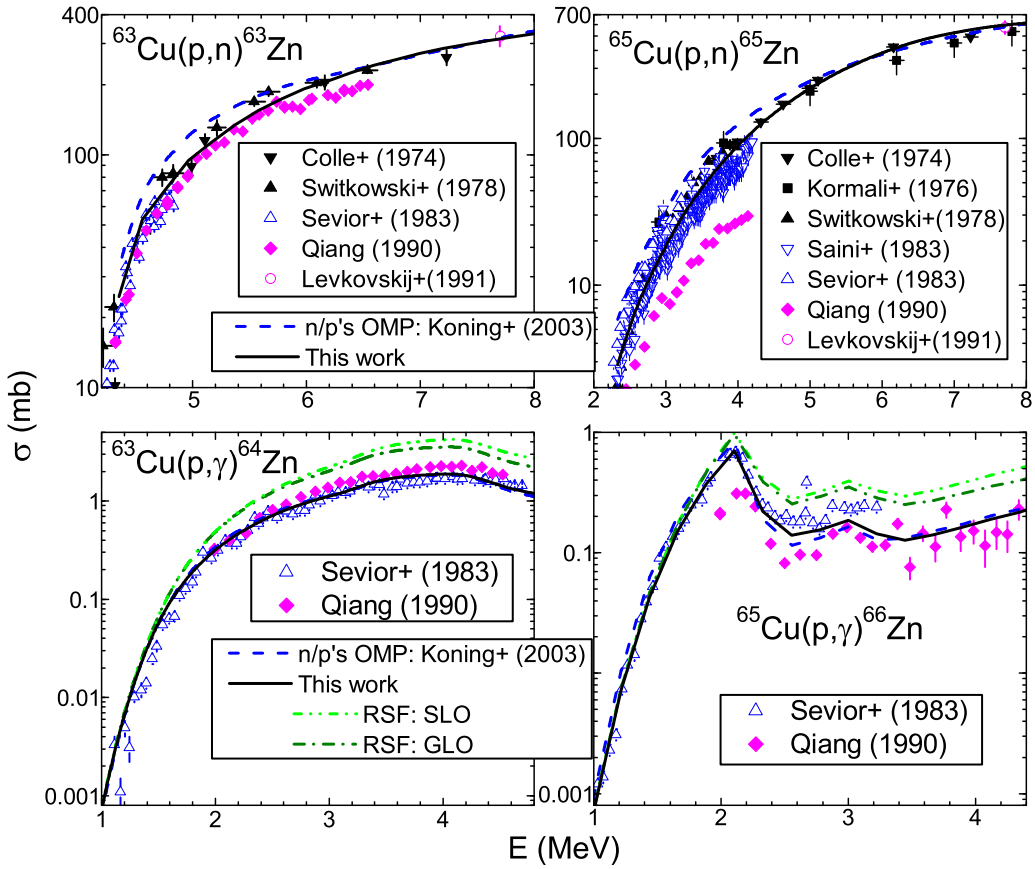

FIG. 1. Comparison of the measured (p,n) and (p,γ) reaction cross sections for ^{63,65}Cu target nuclei [26] and calculated values using the proton OMP parameters of either the local set for ^{63}Cu of Ref. [24] (dashed curves) or finally adopted [46] (solid curves), with addition in the latter case of the results for the (p,γ) reaction corresponding also to the SLO (dash-dot-dotted curves) and GLO (dash-dotted curves) RSF models for $E1$ radiations.

a previous study showed that the few measured proton total reaction cross sections σ_R available for these isotopes at energies around 10 MeV [44] are overestimated (Fig. 2 of Ref. [45]). Therefore, an analysis of the (p,n) reaction cross sections was carried out within several MeV above the (p,n) reaction effective thresholds for ^{63,65}Cu target nuclei, with the results shown in Fig. 1.

The corresponding SM calculations were obviously carried out using the same input parameters as in the rest of this work and a similar one for Zn isotopes [20], except that DI inelastic-scattering cross sections of only several percent for the proton energies up to 8 MeV were taken into account for the decrease of the σ_R finally involved within CN calculations. We found thus a ∼40% overestimation (dashed lines in Fig. 1) of the measured data [26], especially in the first 2–3 MeV of these excitation functions. It is also visible [40] for the evaluated cross sections of the TENDL-2015 library [41]. This overestimation has been removed (Fig. 1) by using in the present work a local OMP for the low-energy protons on the Cu isotopes [46]. Following also the results shown in Sec. III A, the global potential [24] for protons was used for the other target nuclei within this work.

The α-particle optical potential for nuclei within the $45 \leqslant A \leqslant 209$ range [7] has been used for both α-induced reaction and α-emission calculations, following the conclusions corresponding to the $A \sim 60$ nuclei [20].

The same OMP could be also involved in DI distorted-wave Born approximation (DWBA) calculation of the cross sections for the collective inelastic scattering, using the corresponding deformation parameters of the first 2^+ and 3^- collective states, and the CE collective form [20,23]. This approach should be involved prior to model calculations with SM codes such as STAPRE-H, while a similar method is the default one within the complex code TALYS. However, typical DI inelastic-scattering cross sections, taken into account for the decrease of the α-particle σ_R within the CN calculations for, e.g., the target nucleus ^{60}Ni, grow from ∼1% to <6% of σ_R for α-particle energies from 5 to 7.6 MeV and then decrease. Therefore, this correction has not been systematically taken into account in the present work, with no real effect on the calculated reaction cross sections [23], while additional comments related to the use of TALYS are given in Sec. III C 2.

3. *γ-ray strength functions*

Contrary to the use of γ-ray strength functions established by a renormalization carried out in order to achieve agreement with the (α,γ) data (e.g., Ref. [2]), we rely on the measured

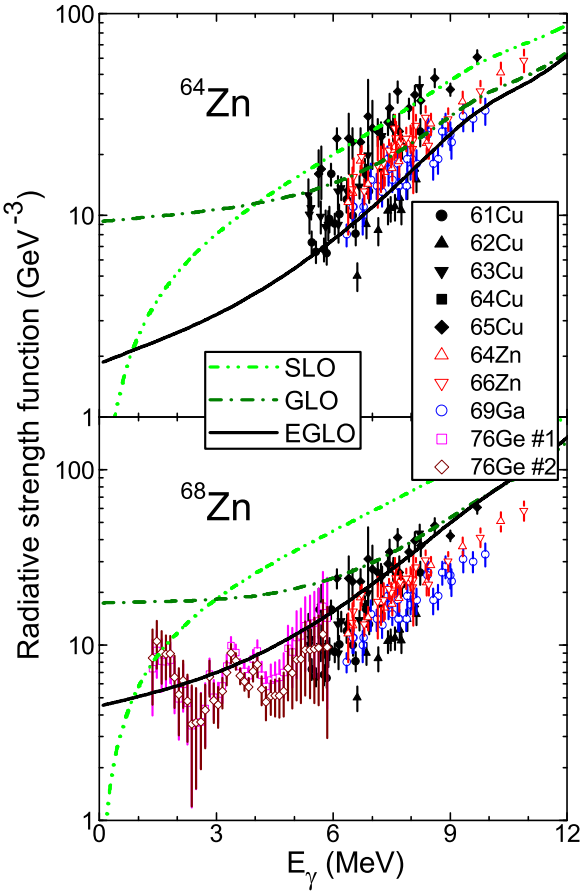

FIG. 2. Comparison of the sum of calculated γ-ray strength functions of the $E1$ and $M1$ radiations for ^{64}Zn and ^{68}Zn nuclei, using to the SLO (dash-dot-dotted curves), GLO (dash-dotted curves), and EGLO (solid curves) models for $E1$ radiations and the SLO model for $M1$ radiations. Also shown are the measured dipole γ-ray strength functions for ^{61,62,63,64,65}Cu, ^{64,66}Zn, ^{69}Ga, and ^{76}Ge nuclei [27–33].

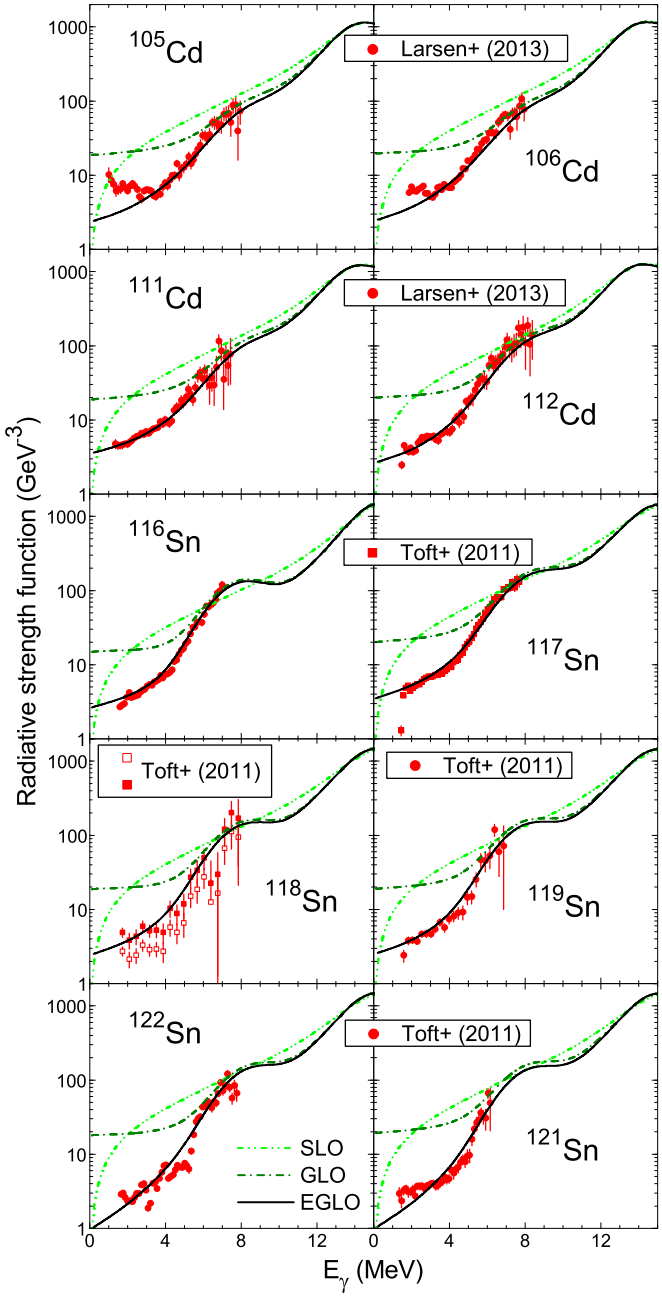

FIG. 3. As Fig. 2 but for ^{105,106,111,112}Cd [34] and $^{116-119,121,122}$Sn [35] nuclei.

data of radiative strength function (RSF) and average s-wave radiation widths Γ_γ [38] (Table I). Used in this respect are the formerly measured RSFs [27–32] and one high-accuracy measurement at lower energies [33] in the neighborhood of the compound nuclei around $A \sim 60$, and the recent systematic analyzes for Cd [34] and Sn [35] isotopes, around $A \sim 110$. An analysis of similar data for heavier nuclei [36] was already provided previously [7].

Moreover, the electric-dipole γ-ray strength functions, of main importance for calculation of the γ-ray transmission coefficients, have been described by using the former Lorentzian (SLO) [47], generalized Lorentzian (GLO) [48], and enhanced generalized Lorentzian (EGLO) [49] models. A constant nuclear temperature T_f of the final states [50] has been particularly used within the EGLO model. The giant dipole resonance (GDR) line-shape usual parameters have been derived from photoabsorption data, while the SLO model was used for the $M1$ radiation, with the global parametrization [38] for the GDR energy and width, i.e., $E_0 = 41/A^{1/3}$ MeV and $\Gamma_0 = 4$ MeV. Further details on particular parameter values are given hereafter.

Comparison of the measured and calculated sum of γ-ray strength functions of the $E1$ and $M1$ radiations for the nuclei of interest within present work with $A \sim 60$ (Fig. 2) and $A \sim 110$ (Fig. 3), similarly to Fig. 3 of Ref. [7] for $A \sim 160$, proves that both the SLO and GLO models overestimate the RSF data below the nucleon binding energy for all these mass ranges. The calculated Γ_γ values corresponding to these γ-ray strength functions are also given in Table I for each $E1$ model involved in the present work. They are compared to the values either measured or deduced from systematics of the measured-data dependence on the neutron separation energy S.

In spite of the low accuracy of these estimations for $A \sim 60$ nuclei, only the EGLO γ-ray strength functions may provide values closer to the measured data. Moreover, just the same functions show a rather constant nonzero limit, which is comparable to an average of the recent RSF data obtained for ^{74,76}Ge nuclei [33]. It is true that the agreement of the measured and calculated values with the EGLO model for $E1$ radiation is obtained even in the limit of 2σ uncertainty of the former. However, it is generally much better than in the case of the SLO and GLO models which may provide calculated values several times larger than the measured ones. Similar results were obtained previously for the heavier nuclei (Figs. 2–3 of Ref. [7]) while they are of less interest for the present discussion of the only recent (α,n) data for ^{164,166}Er and ^{187}Re target nuclei, at energies well above threshold.

(p,γ) reaction data analysis for ^{63,65}Cu isotopes (Fig. 1) has additionally been used to check the accuracy of the adopted RSFs for $A \sim 60$ nuclei. Actually, the RSF uncertainties corresponding even to the EGLO model are largest for this mass range, in the absence of any detailed GDR and RSF recent study, as in the case of the heavier nuclei. Thus, the GDR parameters derived from photoabsorption data for ^{64}Zn [31] and ^{70}Ge [51] have been used for ^{62,64,65,66}Zn and ^{68}Zn excited nuclei, respectively. Finally, we adopted a $T_f = 0.7$ MeV parameter value and a GDR peak cross section of 1.5 mb for the $M1$ radiation in order to obtain a compromise between the account of the RSF and Γ_γ data as well (Fig. 2).

In spite of this rather rough EGLO approach, the comparison of the experimental and calculated (p,γ) reaction data for ^{63,65}Cu pointed out, however, a good agreement for the use of this option. While the measured data are well described by the parameters adopted in the present work, one may note a calculated cross-section increase of even a factor >2 for the incident energies above the (p,n) reaction threshold if the EGLO model is replaced by the GLO one. A slightly larger factor is given by the use of the SLO model, which shows particularly that the RSF values at γ energies larger than ~3 MeV are more important for the calculation of capture cross sections. Thus it results that an eventual low-energy RSF enhancement [33], if it exists for any of the Zn isotopes, would not affect essentially the calculated (p,γ) reaction cross sections.

III. RESULTS AND DISCUSSION

A. (α,x) reactions for stable Ni isotopes

The former version [9] of the actual α-particle potential [7] provided a suitable description at once of all (α,γ), (α,n), and (α,p) reaction data available at that time for ^{58,62,64}Ni and energies below $\sim 0.6B$, $0.8B$, and $0.7B$, respectively, where $B = 2.88Z/(2.66 + 1.36A^{1/3})$ MeV is the Coulomb barrier [52] corresponding to the fitted experimental interaction radii. The new high-precision data [1,13,14] are particularly worthwhile for the present work as they (i) enlarge the corresponding energy range even above $0.8B$ for the three above-mentioned isotopes, (ii) provide the first measured (α,γ) reaction cross section for ^{60,61}Ni, and (iii) make possible a complete view of the (α,x) reaction cross sections below B for a significant chain of stable isotopes (Fig. 4).

Because similar if not identical consistent input-parameter sets have formerly as well as presently been involved, the rather good agreement of all measured and calculated data shown in Fig. 4 is not surprising. The more important replacement of an early $E1$ model used in the past [9] has little effect on the calculated cross sections as the corresponding former predictions were also checked versus the RSF and Γ_γ data. Nevertheless, one may consider that the presently improved approach has led to the better description of the excitation-function structure above the (α,n) reaction threshold for ^{62,64}Ni target nuclei.

On the other hand, the above comments concerning the RSF effects on the calculated (p,γ) reaction cross sections are suitable for these (α,γ) reactions as well, except for the differences between the values obtained by using the various models. Thus, the use of the GLO model provides values larger by ~50% than the results related to the EGLO model, while a rather similar increase is additionally provided by the SLO model. This trend could be related to a slightly different γ-ray range involved within the decay of the same CNs populated by either protons or α particles, all above the energy of 3–4 MeV (below which the RSFs given by the SLO model are increasingly lower than the GLO values). The region just above this energy is involved in the case of the (p,γ) reactions, while higher energies (but yet below the nucleon binding energies) play a more significant role for the (α,γ) reactions. The most important point for the present work is still the consequent conclusion that an eventual low-energy RSF enhancement [33] would not affect essentially the calculated (α,γ) reaction cross sections.

The systematic study of the (α,γ) reactions for stable Ni isotopes [1] makes possible a more sensitive comparison of the results corresponding to the global α-particle potentials of Refs. [7,17] as well as the advantage provided by this study versus that of the much-larger (α,p) and (α,n) reaction cross sections. Thus, the calculated results of the (α,γ) reaction definitely show cross sections increased by 50–100% at the lowest incident energies but 10–20% lower above 9 MeV, corresponding to a lower slope of the excitation function given by the potential of McFadden and Satchler [17]. This latter potential definitely works very well for an OMP having only four constant parameters and no surface imaginary component, except, however, for the lowest energies of largest interest for nuclear astrophysics and fusion technology.

On the other hand, the accuracy of these calculated (α,γ) reaction cross sections is not affected by an eventual less suitable knowledge of the nucleon OMPs. This has been found by replacing the above-mentioned OMPs by those of Koning and Delaroche [24], for the proton- and neutron-rich ^{58,64}Ni target nuclei, with the (α,p) and (α,n) reaction cross sections being the largest fraction of the total reaction cross section, respectively. In spite of the above-mentioned (Sec. II B 2) large differences between the nucleon OMPs adopted within this work for the Zn and Cu target nuclei, and Ref. [24], the (α,γ) reaction cross sections have been changed by less than 15% through the use of the alternate OMPs. A larger decrease up to 23% was obtained only around the minimum of the ^{64}Ni$(\alpha,\gamma)^{68}$Zn excitation function just above the (α,n) reaction threshold.

Concerning the relation of the recent studies of the (α,γ) reactions for Ni isotopes [1,13,14] and present conclusions

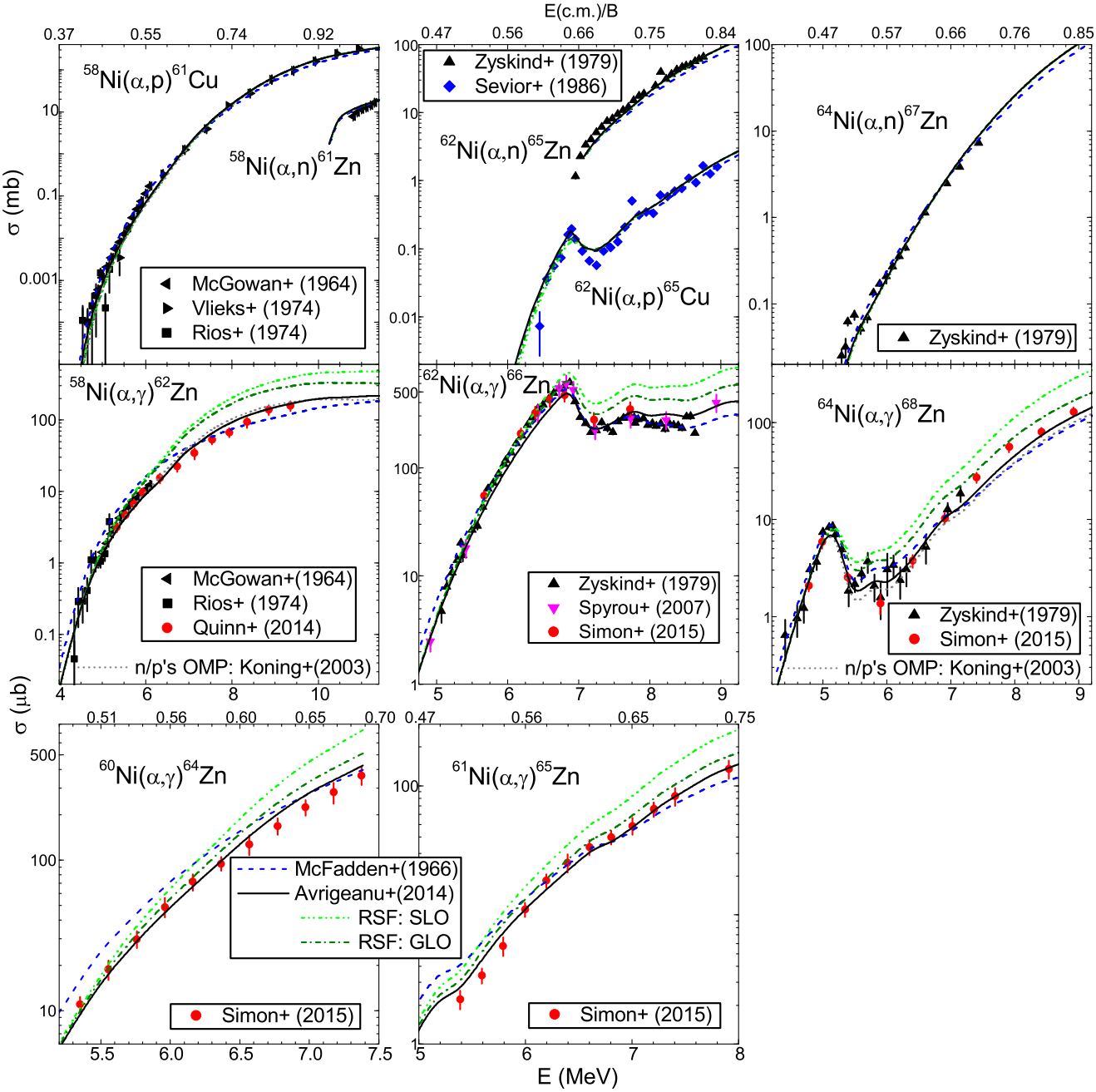

FIG. 4. Comparison of the measured α-induced reaction cross sections for $^{58,60-62,64}$Ni target nuclei [1,26] and calculated values using the α-particle global OMPs of either Ref. [17] (dashed curves) or Ref. [7] (solid curves), and with the alternate involvements for the latter OMP of either the GLO (dash-dotted curves) and SLO (dash-dot-dotted curves) RSF models, or the nucleon OMPs [24] (short-dotted curves), vs laboratory energy of α particles (bottom) and corresponding ratio of the center-of-mass energy and the Coulomb barrier B [52] (top).

on the α-particle potentials and RSF models, one may note the following point. The combination of input parameters for the TALYS 1.6 code [15] that reproduced simultaneously the experimental data for all Ni isotopes [1] includes a potential which is the simpler version of the α-particle OMPs of Ref. [16]. However, the more complete and physical one, which is the third potential of that work, was found [14] to be most suitable for ^{62}Ni. Also, the RSF which was found to be most suitable for ^{60,62}Ni isotopes belongs to the GLO model, at variance with the RSF data shown in the present work. Therefore, compensation effects of less suitable options for various SM parameters cannot be avoided, contrary to the use of a consistent parameter set.

B. (α,x) reaction data analysis for $A \sim 110$ nuclei

The recent RSF data of the Cd and Sn nuclei and their sensible analysis [34,35] have allowed a notably improved study of the (α,γ) reaction cross sections on $A \sim 110$ nuclei. Because it is commonly assumed that there is a small difference

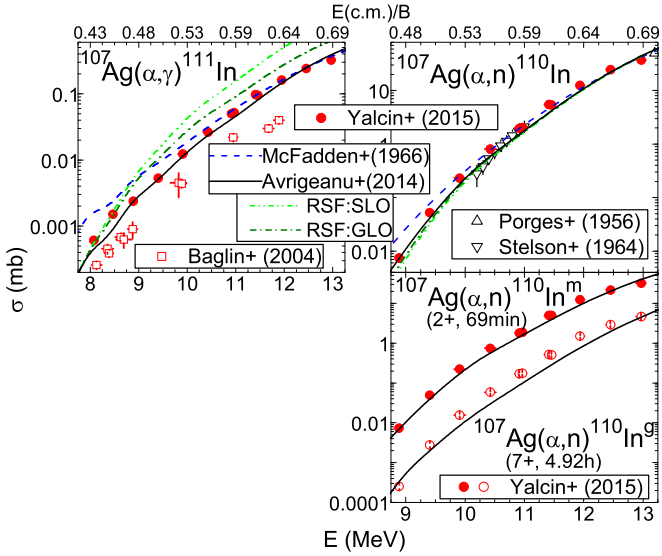

FIG. 5. As Fig. 4 but for ^{107}Ag [2,26,53].

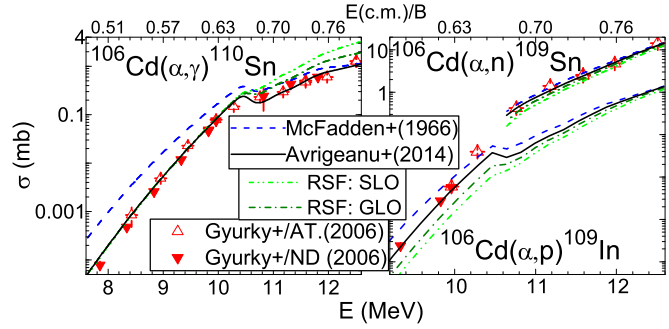

FIG. 6. As Fig. 4 but for ^{106}Cd [26].

in the RSFs of neighboring isotopes, we have used GDR, pygmy resonance, and T_f parameters within the EGLO model obtained for some of these nuclei, as mentioned below. Actually, the use of the new RSF approach and the updated level-density parameters (Table I) are the changes within this work with reference to our previous analysis for ^{106}Cd [9] and ^{112}Sn [19] using the former version [9] of the actual potential.

1. ^{107}Ag

The high-precision measured data for ^{107}Ag [2] have completed the earlier data available, especially for the (α,n) reaction. On the other hand, a disagreement of these data for the (α,γ) reaction with a set only a decade older [53] means a further analysis would be useful. In this respect, we have considered that the use of the EGLO parameters [34], found to describe quite well the RSF data for ^{111}Cd (see also Fig. 3), should be suitable also for ^{111}In. An additional support for using these parameters comes from a very recent study of RSFs in the ^{114}Cd(γ,γ') and ^{113}Cd(n,γ) reactions [54], which found similar experimental RSF values for ^{114}Cd and ^{112}Cd [34] above 7 MeV. However, a difference at lower energies was found, which was attributed also to the spin distribution of the states excited through the $(^3\mathrm{He},^3\mathrm{He}')$ and (γ,γ') processes. Therefore, the RSF data and parameters obtained by the Oslo group [34,35] are particularly suitable for the analysis of (α,γ) reactions.

The general agreement between the present calculations and the measured data for this target nucleus (Fig. 5) has been obtained by using no rescaling factor or change of the α-particle potential [7]. There is only a slight underestimation of the 7^+ ground state of the residual nucleus ^{111}In which could be also due to the knowledge of the corresponding decay scheme. On the other hand, a similar underestimation but for the lowest two measured points of the (α,γ) reaction may follow the use of a 0.2-MeV equidistant binning for the excitation energy grid. Beyond the validation of the α-particle potential [7], these results may additionally confirm the latest measured data set for the (α,γ) reaction [2] with respect to the former one [53].

2. ^{106}Cd

A recent measurement and analysis of α-particle elastic scattering angular distributions on ^{106}Cd in the wide energy range from 16.1 to 27 MeV has been accompanied by a discussion of the α-induced reaction cross sections below 12 MeV [3]. The worthy analysis of the scattering angular distributions included also former data and the ATOMKI-V1 global potential [55] based entirely on elastic scattering data in the $89 \leqslant A \leqslant 144$ range, around B. A final remark of this work stated that conclusions on the α-particle potential from the α-induced reaction data are difficult in the case of this nucleus. The potential devoted particularly to heavy nuclei [10] was used in the elastic scattering analysis, on the correct premise that the latest version [7] would provide similar results. However, the former potential was used also within the reaction data analysis, where the same assertion became wrong. Nevertheless, mainly a large underestimation of the (α,p) reaction cross sections [3], related to the use of this potential, has triggered the following assay.

Actually, the same reaction data were already fully described by the former version of this potential (Fig. 15 of Ref. [9]). The basic point of the present calculation has been the use of the RSF parameters of ^{106}Cd [34], with the same above-mentioned motivation of close neighborhood of the corresponding compound nucleus ^{110}Sn. The agreement of the calculated and measured data (Fig. 6) is again quite similar to that shown earlier [9], but now we point out the RSF effects on the calculated (α,γ) as well as (α,p) reaction cross sections. In fact, the negligible size of these effects for the dominant (α,γ) reaction below the particle-emission threshold stands as a major advantage of this reaction at similar energies for the α-particle OMP study. On the other hand, at the same energies the minor (α,p) reaction cross sections decrease by factors of 2–3 and 3–5, respectively, when the EGLO model is replaced by the GLO and SLO options. Then, above the (α,n) reaction threshold, the increase of the calculated (α,γ) reaction cross sections, by additional factors of $\sim$2 for the same changes, as well as a reducing decrease of the (α,p) reaction cross sections, follow naturally the corresponding RSFs. Therefore, the real cause of the (α,p) reaction data underestimation below and around the (α,n) reaction threshold [3] has been not the

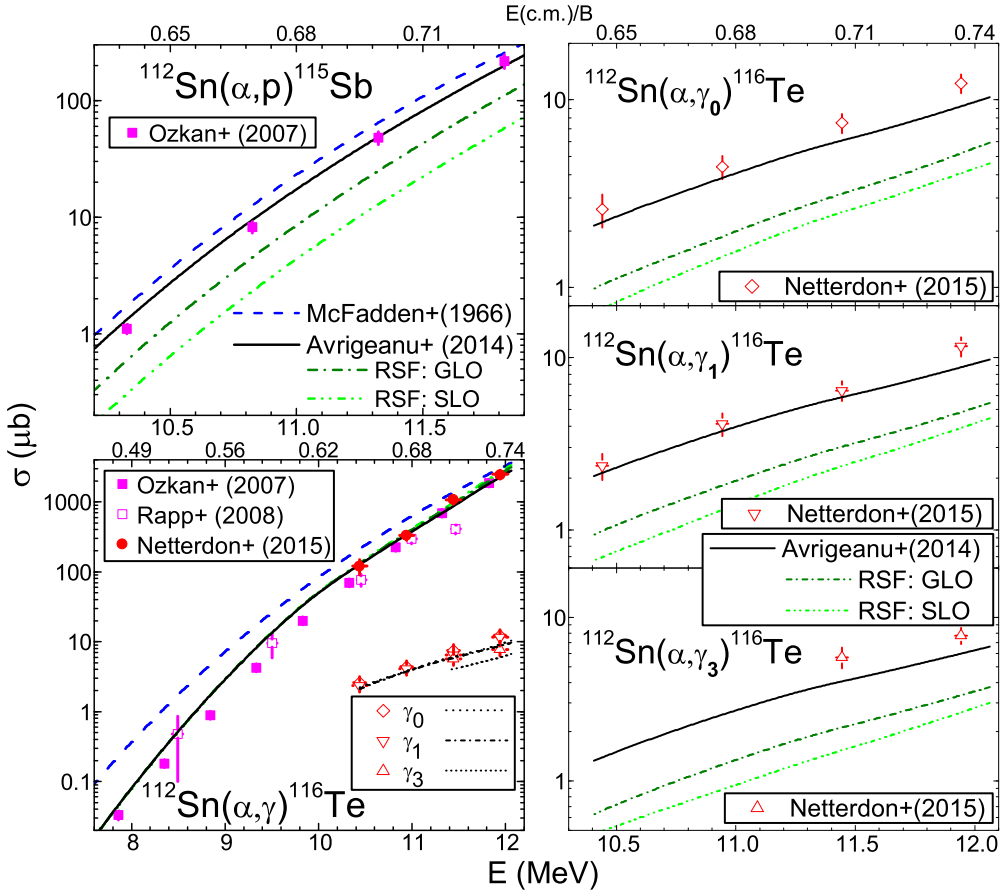

FIG. 7. As Fig. 4 but for ^{112}Sn [4,26] and the partial (α,γ) reaction cross sections for the decay of the entry state to the ground state and the first and the third excited states of the residual nucleus ^{116}Te.

α-particle potential but a deficient RSF involved within the SM analysis.

On the other hand, the above-mentioned analysis [3] noted the use of cross-section ratios like $\sigma(\alpha,p)/\sigma(\alpha,\gamma)$ and $\sigma(\alpha,n)/\sigma(\alpha,\gamma)$ as an excellent measure for the further ingredients of SM calculations beyond the α-particle OMP [56]. However, this ratio method is less relevant for the present work since, first, all main ingredients have been fixed independently, and, second, a rather good agreement of the measured and calculated data has been obtained for each reaction channel. Moreover, it was also shown that this method may provide an eventual scaling factor only for the ratios T_p/T_γ or T_n/T_γ of the nucleons and γ-ray transmission coefficients [56].

3. ^{112}Sn

A similar relation between the (α,γ) and (α,p) reaction cross sections, at incident energies below the (α,n) reaction threshold, exists also for the proton-rich ^{112}Sn target nucleus. The data measured for these reactions before 2010 were also suitably described [9,19] while a new measurement of the (α,γ) reaction cross sections [4] removes a minor discrepancy between two earlier data sets and actually has strengthened the validation of the present potential (Fig. 7). The RSF parameters of ^{112}Cd [34] have been used in this respect, with the following comment.

The analysis within Ref. [4] had to assume several parameter adjustments [4] including a reduction by a factor of 0.2 for the proton width provided by a default TALYS calculation, i.e., using the global nucleon optical potentials [24], in order to describe the data for ^{112}Sn. Then, a major underestimation of the (α,p) reaction cross section for ^{106}Cd was obtained by using the same local parameters [4]. This underestimation was obviously following the hard reduction factor of 0.2 adopted for the proton width while the global proton optical potential [24] was proved independently to work quite well in this mass region [19]. On the contrary, no scaling factor has been requested by the agreement shown in Fig. 7 also for the (α,p) reaction. Thus, one may note the concurrent description of the (α,p) reaction data for both target nuclei ^{106}Cd and ^{112}Sn, with no change of the OMPs and/or RSF parameters. Moreover, even the changes of the calculated cross sections of this reaction, due to the use of alternate RSF models GLO and SLO, show nearly the same ratios (Fig. 7) as in the above case of ^{106}Cd (Fig. 6).

Nevertheless, the main achievement of Ref. [4], namely the first measurement of partial (α,γ) cross sections, has made possible a really sound check of the adopted RSFs, beyond that of the α-particle potential. The calculated partial cross sections shown in Fig. 7 correspond only to the side feeding of the corresponding ground and excited states. The comparison of the experimental and calculated partial cross sections validated

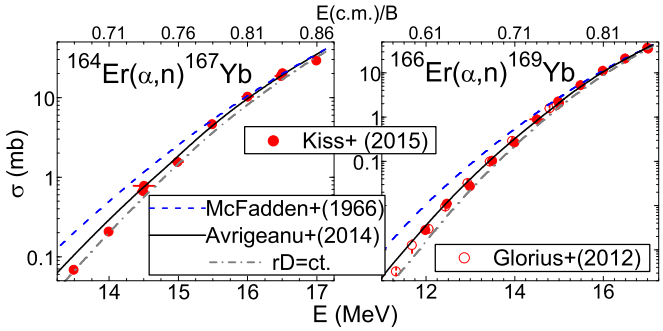

FIG. 8. Comparison of recently measured (α,n) reaction cross sections for ^{164,166}Er [5,57] with the calculated values using the α-particle OMPs of Refs. [17] (dashed curves) and [7] with (solid curves) as well as without (dash-dotted curves) the energy-dependent radius for the lower-energy surface imaginary potential of the well-deformed nuclei.

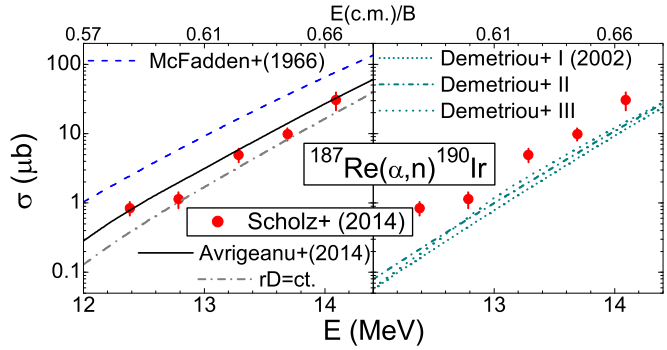

FIG. 9. As Fig. 8 but for ^{187}Re [6] (left), and the OMPs I–III of Ref. [16] (short dotted, short dash-dotted, and short dashed curves, respectively) (right).

actually the whole SM approach as well as its two main ingredients for the present topic.

C. (α,x) reaction data analysis for well-deformed nuclei

The (α,n) reaction cross-section studies performed in the meantime for the heavier nuclei ^{164,166}Er [5] and ^{187}Re [6] made possible a further check of the previous inference of ∼7% larger, at the lowest energies, as well as energy-dependent radius of the surface imaginary part of the α-particle potential for the well-deformed nuclei [7].

1. ^{164,166}Er

The more recent (α,n) reaction data for ^{166}Er [5] are compared with the calculation results and the former data [57] (Fig. 8). The same SM parameters, which were so recently already assessed, were used for the new data analysis, too. The calculated cross sections have been obtained without as well as with the energy-dependent radius r_D for the surface imaginary potential of the well-deformed nuclei [7]. The additional data for ^{166}Er show an even better agreement with the results corresponding to the energy-dependent r_D quantity. A good agreement of the measured [5] and the final values of calculated cross sections for ^{164}Er has also been obtained except the two lowest-energy points (Fig. 8). However, the agreement would exist even for these points if their energy-error bars would be similar to the next point at 14.51 MeV [5]. Moreover, for a broader overview, it could be noted the good agreement of the calculated and measured data for all Er isotopes as well (Fig. 8 of Ref. [40]).

On the other hand, the main conclusion of Ref. [5], concerning the confirmed necessity of an energy-dependent modification of the α-particle potential at very low energies, strengthens the assumed [9] and validated [7,10,20] energy dependence of the surface imaginary-potential depth below as well as above $0.9B$.

2. ^{187}Re

The target nucleus ^{187}Re [6] is quite interesting due to its place at the side of the well-deformed nuclei region. So, it has been of real interest to check in this case the assumption of an energy-dependent increased r_D radius below and around B, for the well-deformed nuclei.

The corresponding (α,n) reaction cross sections (Fig. 9) have also been obtained with the code TALYS. Following large-scale calculations [58], the global potential [7] is stated as its default option for α particles (Ref. [15], p. 9) but use of the corresponding specific option is still necessary in order to have it involved. The calculated cross sections obtained with the code STAPRE-H are larger by 5–9% in the energy range of the measured data [6]. While it has been shown recently that different codes may lead to significantly discrepant results [59], the grounds of the above-mentioned differences can be noticed more easily by using several TALYS options.

A first point which should be made clear, next to the discussion at the end of Sec. II B 2, is the contribution of the direct inelastic scattering, which is by default provided by TALYS. It varies between from 0.03 to 0.17% in the energy range of the measured data [6], so that its absence from the present STAPRE-H analysis cannot motivate the larger (α,n) reaction cross sections. Moreover, no change of the calculated (α,n) reaction cross sections has been obtained by not using the TALYS-1.8 logarithmic binning of the excitation energy grid but equidistant ones, with bin size going from rather half of the one used in calculation with STAPRE-H to nearly twice the latter. So low sensitivity is certainly related to the smaller excitation energies for the present reaction data, up to 14 MeV, while the improvement of the calculated results due to a logarithmic binning is significant especially above 100 MeV [15]. On the other hand, the same differences exist between the calculated σ_R using the two codes, while the ratio of (α,n) reaction cross section and σ_R increases from ∼95 to 99% with the incident energy for these measured data [6].

Actually, the OM code SCAT2 [60] is used within STAPRE-H whereas the OM and coupled-channels code ECIS-06 (see Ref. [15]) is transformed into a subroutine of TALYS. Following the previous comparison of the σ_R values obtained with the SCAT2000 and ECIS96 codes for nucleons [38], we compared the TALYS result with that of the SCAT2 sample case for α-particles on ^{238}U [60], at 13 MeV in the center-of-mass system, and found a difference of ∼5.5%. Therefore it results that the calculated cross sections with the codes STAPRE-H and TALYS

are different due to the OM subroutines of the two codes. However, since these differences are yet 2–3 times smaller than the weighted uncertainties of the accurate data [6], we have considered the results of both codes to be reliable. Nevertheless, further consideration should concern the origin of the discrepancies between the SCAT2000 and ECIS96 results, which remain beyond the scope of this paper due to their reduced significance for the actual questions on the α-particle OMP [1–6].

The calculated cross sections correspond to the constant as well as increased and energy-dependent r_D radii (Fig. 9). It is amazing how the first measured cross sections of this reaction [6] are just in between the calculated cross sections related to the well-deformed and spherical nuclei, respectively, but closer to the former results.

One may note that the presently calculated data for ^{166}Er and ^{187}Re have been obtained by using the same α-particle global potential [7]. On the contrary, the energy-dependence steepness assumed for the Fermi-type volume imaginary potential had different parameter values of 2.5 [61] and 4 MeV [6], respectively.

Because the analysis of Ref. [6] involved also the first of the three global OMPs by Demetriou *et al.* [16], which was identified as the α-particle OMP that reproduces simultaneously the experimental data for all Ni isotopes [1] while the more complete and physical version is the third potential of the same authors; the results corresponding to all three potentials [16] are also shown in Fig. 9. The larger underestimation of the measured data [6] by the first potential of Demetriou *et al.* is somehow reduced but not fully removed by using particularly their third potential.

IV. CONCLUSIONS

Recent high-precision (α,x) reaction data for the target nuclei $^{58,60-62,64}$Ni [1], ^{107}Ag [2], ^{106}Cd [3], ^{112}Sn [4], ^{164,166}Er [5], and ^{187}Re [6] have been analyzed in order to investigate the reliability of SM predictions on the basis of a previous α-particle global potential [7]. While the description of the (α,γ) as well as of the (α,n) and (α,p) reactions was problematic within the above-mentioned original studies, a careful assessment of the related model parameters was first undertaken in the present work. This goal was achieved through various independent data analysis. Thus, the transmission coefficients of nucleons and γ rays, given by the corresponding optical potentials and γ-ray strength functions, respectively, have particularly been fixed by independent analysis of (p,n) reaction and radiative strength function data. Then, they have also been checked by means of (p,γ) reaction data. As a result, the accurate (α,x) reaction data became particularly sensitive to the α-particle optical potential.

There are several critical features of the statistical model parameters which led to particular conclusions of the present work. The γ-ray energies larger than $\sim$3 MeV are more important for the calculation of the (p,γ) reaction cross sections, while higher energies (but yet below the nucleon binding energies) play a more significant role for the (α,γ) reactions. Therefore, it results that an eventual low-energy RSF enhancement [33] would not affect essentially the calculated (α,γ) reaction cross sections.

On the other hand, comparison with the results which have been obtained by using alternate parameters, particularly for α-particle optical potential and RSFs, has shown that compensation effects of less suitable options of various SM parameters cannot be avoided unless a consistent parameter set is used. Thus it has also been possible to point out that the real cause of the (α,p) reaction data underestimation below and around the (α,n) reaction threshold, for the proton-rich nuclei ^{106}Cd and ^{112}Sn, has been not the α-particle potential but a deficient RSF involved within the SM analysis. Actually, the largest importance of the RSF models for the suitable evaluation of the nucleon-capture cross sections has already been pointed out within, e.g., the detailed studies of Beard *et al.* [62]. They have shown that the knowledge of RSFs is in that case even more crucial than information on nucleon OMPs.

The suitable description of all these recent reaction data has been proved possible with no empirical rescaling factors of the γ and/or nucleon widths. It should be considered together with the earlier data for nuclei in the whole range $45 \leqslant A \leqslant 209$ which were involved within the assessment of the present optical potential [7,9,10]. Moreover, the agreement of the new measured and calculated (α,x) reaction cross sections proves the correctness of both the α-particle global optical potential [7] itself and its setting up below B. Indeed, at these energies it was fully based on various SM calculations [7,9,10], which were carried out using consistent sets of SM parameters. Furthermore, its validation for the α-particle emission in proton-induced reactions on Zn isotopes [20] should be extended over the same A range as for the incident channel in order to prove fully a global character.

ACKNOWLEDGMENT

This work was partly supported by Fusion for Energy (F4E-GRT-168-02) and by Autoritatea Nationala pentru Cercetare Stiintifica (PN-42160102).

[1] A. Simon *et al.*, Phys. Rev. C **92**, 025806 (2015).
[2] C. Yalçin *et al.*, Phys. Rev. C **91**, 034610 (2015).
[3] A. Ornelas *et al.*, Nucl. Phys. A **940**, 194 (2015).
[4] L. Netterdon, J. Mayer, P. Scholz, and A. Zilges, Phys. Rev. C **91**, 035801 (2015).
[5] G. G. Kiss, T. Szücs, T. Rauscher, L. Csedreki, Zs. Fülöp, Gy. Gyürky, and Z. Halász, J. Phys. G: Nucl. Part. Phys. **42**, 055103 (2015).
[6] P. Scholz *et al.*, Phys. Rev. C **90**, 065807 (2014).
[7] V. Avrigeanu, M. Avrigeanu, and C. Mănăilescu, Phys. Rev. C **90**, 044612 (2014).
[8] M. Avrigeanu, W. von Oertzen, A. J. M. Plompen, and V. Avrigeanu, Nucl. Phys. A **723**, 104 (2003).
[9] M. Avrigeanu, A. C. Obreja, F. L. Roman, V. Avrigeanu, and W. von Oertzen, At. Data Nucl. Data Tables **95**, 501 (2009).
[10] M. Avrigeanu and V. Avrigeanu, Phys. Rev. C **82**, 014606 (2010).

[11] E. Somorjai *et al.*, Astron. Astrophys. **333**, 1112 (1998).
[12] A. Sauerwein *et al.*, Phys. Rev. C **84**, 045808 (2011).
[13] S. J. Quinn *et al.*, Phys. Rev. C **89**, 054611 (2014).
[14] A. Spyrou, H.-W. Becker, A. Lagoyannis, S. Harissopulos, and C. Rolfs, Phys. Rev. C **76**, 015802 (2007).
[15] A. J. Koning, S. Hilaire, and M. C. Duijvestijn, TALYS-1.0, in *Proceedings of the International Conference on Nuclear Data for Science and Technology, Nice, 2007*, edited by O. Bersillon, F. Gunsing, E. Bauge, R. Jacqmin, and S. Leray (EDP Sciences, Paris, 2008), p. 211; versions TALYS-1.6, Dec. 2013; TALYS-1.8, Jan. 2016 [http://www.talys.eu; http://www.talys.eu/fileadmin/talys/user/docs/talys1.8.pdf].
[16] P. Demetriou, C. Grama, and S. Goriely, Nucl. Phys. A **707**, 253 (2002).
[17] L. McFadden and G. R. Satchler, Nucl. Phys. A **84**, 177 (1966).
[18] T. Rauscher, Phys. Rev. Lett. **111**, 061104 (2013).
[19] M. Avrigeanu and V. Avrigeanu, Phys. Rev. C **79**, 027601 (2009).
[20] V. Avrigeanu and M. Avrigeanu, Phys. Rev. C **91**, 064611 (2015).
[21] C. Mănăilescu, Rom. Rep. Phys. **68**, 169 (2016).
[22] V. Avrigeanu, M. Avrigeanu, and C. Mănăilescu, AIP Conf. Proc. **1645**, 148 (2015); http://cssp14.nipne.ro.
[23] V. Avrigeanu, M. Avrigeanu, and C. Mănăilescu, arXiv:1605.05455v1 [nucl-th].
[24] A. J. Koning and J. P. Delaroche, Nucl. Phys. A **713**, 231 (2003).
[25] H. Vonach, M. Uhl, B. Strohmaier, B. W. Smith, E. G. Bilpuch, and G. E. Mitchell, Phys. Rev. C **38**, 2541 (1988).
[26] Experimental Nuclear Reaction Data (EXFOR) [http://www-nds.iaea.org/exfor/].
[27] K. Nilson, B. Erlandsson, and A. Marcinkowski, Nucl. Phys. A **391**, 61 (1982).
[28] K. Nilson, B. Erlandsson, and A. Marcinkowski, Nucl. Phys. A **348**, 1 (1980).
[29] T. Belgya *et al.*, Tech. Rep. IAEA-TECDOC-1506, IAEA, Vienna, Austria, 2006 (unpublished), p. 97 [https://www-nds.iaea.org/publications/tecdocs/iaea-tecdoc-1506/].
[30] B. Erlandsson, K. Nilson, A. Marcinkowski, and J. Piotrowski, Z. Physik **293**, 43 (1979).
[31] B. Erlandsson, K. Nilson, and A. Marcinkowski, Nucl. Phys. A **343**, 197 (1980); J. P. Roalsvig, R. N. H. Haslam, and J. L. Bergsteinsson, Can. J. Phys. **38**, 320 (1960).
[32] K. Nilson, B. Erlandsson, L. Spanier, and A. Marcinkowski, Nucl. Phys. A **401**, 460 (1983).
[33] A. Spyrou *et al.*, Phys. Rev. Lett. **113**, 232502 (2014).
[34] A. C. Larsen *et al.*, Phys. Rev. C **87**, 014319 (2013).
[35] H. K. Toft *et al.*, Phys. Rev. C **83**, 044320 (2011).
[36] http://www.mn.uio.no/fysikk/english/research/about/infrastructure/OCL/nuclear-physics-research/compilation/
[37] http://www.nndc.bnl.gov/ensdf
[38] R. Capote *et al.*, Nucl. Data Sheets **110**, 3107 (2009) [http://www-nds.iaea.org/RIPL-3/].
[39] M. Avrigeanu and V. Avrigeanu, IPNE Report NP-86-1995, Bucharest, 1995 (unpublished), and references therein; News NEA Data Bank **17**, 22 (1995).
[40] V. Avrigeanu and M. Avrigeanu, arXiv:1606.06188 [nucl-th].
[41] A. J. Koning and D. Rochman, Nucl. Data Sheets **113**, 2841 (2012); A. J. Koning *et al.*, TENDL-2015: TALYS-based evaluated nuclear data library [https://tendl.web.psi.ch/tendl_2015/tendl2015.html].
[42] V. Avrigeanu, T. Glodariu, A. J. M. Plompen, and H. Weigmann, J. Nucl. Sci. Technol. **39** Sup. 2, 746 (2002).
[43] C. A. Engelbrecht and H. Fiedeldey, Ann. Phys. **42**, 262 (1967); RIPL 800 OMP Index [38].
[44] R. F. Carlson, At. Data Nucl. Data Tables **63**, 93 (1996).
[45] M. Avrigeanu, S. V. Chuvaev, A. A. Filatenkov, R. A. Forrest, M. Herman, A. J. Koning, A. J. M. Plompen, F. L. Roman, and V. Avrigeanu, Nucl. Phys. A **806**, 15 (2008).
[46] S. Saini, G. Singh, A. Chatterjee, S. Kailas, D. D. Karnik, N. Veerabahu, and M. K. Mehta, Nucl. Phys. A **405**, 55 (1983).
[47] P. Axel, Phys. Rev. **126**, 671 (1962).
[48] J. Kopecky and M. Uhl, Phys. Rev. C **41**, 1941 (1990).
[49] J. Kopecky, M. Uhl, and R. E. Chrien, Phys. Rev. C **47**, 312 (1993).
[50] A. C. Larsen and S. Goriely, Phys. Rev. C **82**, 014318 (2010).
[51] http://www-nds.iaea.org/RIPL-3/gamma/
[52] W. Nörenberg, in *Heavy Ion Collisins*, Vol. 2, edited by R. Bock (North–Holland, Amsterdam, 1980).
[53] C. M. Baglin, AIP Conf. Proc. **769**, 1370 (2005).
[54] R. Massarczyk *et al.*, Phys. Rev. C **93**, 014301 (2016).
[55] P. Mohr, G. G. Kiss, Zs. Fülöp, D. Galaviz, Gy. Gyürky, and E. Somorjai, At. Data Nucl. Data Tables **99**, 651 (2013).
[56] G. G. Kiss *et al.*, Phys. Rev. C **88**, 045804 (2013).
[57] J. Glorius *et al.*, Phys. Rev. C **89**, 065808 (2014).
[58] A. J. Koning, Report EFFDOC-1271, OECD/NEA Data Bank, Paris, 2015 (unpublished), http://www.oecd-nea.org/dbdata/nds_effdoc/effdoc-1271.pdf.
[59] J. Pereira and F. Montes, Phys. Rev. C **93**, 034611 (2016).
[60] O. Bersillon, *SCAT2: Un programme de modèle optique sphérique*, Note CEA-N-2227, Commissariat à l'Énergie Atomique, Bruyéres-le-Châtel, 1981 (unpublished) [http://www.oecd-nea.org/tools/abstract/detail/nea-0829/].
[61] G. G. Kiss, T. Szücs, T. Rauscher, Zs. Török, Zs. Fülöp, Gy. Gyürky, Z. Halász, and E. Somorjai, Phys. Lett. B **735**, 40 (2014).
[62] M. Beard, S. Frauendorf, B. Kämpfer, R. Schwengner, and M. Wiescher, Phys. Rev. C **85**, 065808 (2012); M. Beard, E. Uberseder, R. Crowter, and M. Wiescher, *ibid.* **90**, 034619 (2014).